American Mineralogist, Volume 99, pages 1767–1773, 2014

Chromo-alumino-povondraite, $NaCr_3(Al_4Mg_2)(Si_6O_{18})(BO_3)_3(OH)_3O$, a new mineral species of the tourmaline supergroup

Leonid Reznitskii[1], Christine M. Clark[2], Frank C. Hawthorne[2,*], Joel D. Grice[3], Henrik Skogby[4], Ulf Hålenius[4] and Ferdinando Bosi[4,5,*]

[1]Institute of the Earth's Crust, Siberian Branch, Russian Academy of Science, Lermontova str., 128, 664033 Irkutsk, Russia
[2]Department of Geological Sciences, University of Manitoba, Winnipeg, Manitoba R3T 2N2, Canada
[3]Research Division, Canadian Museum of Nature, P.O. Box 3443A, Station "D", Ottawa, Ontario K1P 6P4, Canada
[4]Department of Geosciences, Swedish Museum of Natural History, Box 50007, SE-10405 Stockholm, Sweden
[5]Dipartimento di Scienze della Terra, Sapienza Università di Roma, Piazzale Aldo Moro, 5, I-00185 Rome, Italy

ABSTRACT

Chromo-alumino-povondraite, $NaCr_3(Al_4Mg_2)(Si_6O_{18})(BO_3)_3(OH)_3O$, is a new mineral of the tourmaline supergroup. It is found in metaquartzites of the Pereval marble quarry (Sludyanka, Lake Baikal, Russia) in association with dravite, oxy-chromium-dravite, oxy-dravite, quartz, calcite, chromphyllite, eskolaite, chromite, uvarovite, chromian phlogopite, and pyroxenes of the diopside-kosmochlor series, Cr-bearing tremolite, Cr-bearing titanite, Cr-bearing rutile, and pyrite.

Crystals are green and transparent with a vitreous luster, and exhibit a pale-green streak and conchoidal fracture. Chromo-alumino-povondraite has a Mohs hardness of approximately 7½, and a calculated density of 3.227 g/cm^3. In plane-polarized light, chromo-alumino-povondraite is pleochroic (O = emerald green and E = pale yellowish green) and uniaxial negative: ω = 1.745(5), ε = 1.685(5). Chromo-alumino-povondraite is rhombohedral, space group $R3m$, with the unit-cell parameters a = 16.0277(2), c = 7.3085(1) Å, V = 1625.93(5) Å^3, Z = 3. Crystal-chemical analysis resulted in the empirical structural formula:

$$^{X}(Na_{0.87}Ca_{0.07}\square_{0.04}K_{0.02})_{\Sigma1.00}\ ^{Y}(Cr^{3+}_{2.29}Mg_{0.71})_{\Sigma3.00}\ ^{Z}(Al_{3.04}Mg_{1.54}Cr^{3+}_{1.18}V^{3+}_{0.22}Fe^{3+}_{0.01})_{\Sigma6.00}$$
$$[^{T}(Si_{5.96}Al_{0.04})O_{18}]\ (^{B}BO_3)_3\ ^{V}(OH)_3\ ^{W}[O_{0.73}F_{0.25}(OH)_{0.02}]_{\Sigma1.00}$$

The crystal structure of chromo-alumino-povondraite was refined to an $R1$ index of 1.68% using 1803 unique reflections collected with Mo$K\alpha$ X-radiation. Ideally, chromo-alumino-povondraite is related to oxy-dravite and oxy-chromium-dravite by the homovalent substitution $Cr^{3+} \leftrightarrow Al^{3+}$. Tourmaline with chemical compositions classified as chromo-alumino-povondraite can be either Al-dominant or Cr-dominant as a result of the compositional boundaries along the solid solution between Al and Cr^{3+} that are determined at $^{Y+Z}(Cr_{1.5}Al_{5.5})$, corresponding to $Na^{Y}(Cr_{1.5}Al_{1.5})^{Z}(Al_4Mg_2)Si_6O_{18}(BO_3)_3(OH)_3O$, and $^{Y+Z}(Cr_5Al_2)$, corresponding to $Na^{Y}(Cr_3)^{Z}(Cr_2Al_2Mg_2)Si_6O_{18}(BO_3)_3(OH)_3O$.

Keywords: Chromo-alumino-povondraite, tourmaline, new mineral species, electron microprobe, crystal-structure refinement, infrared spectroscopy, optical absorption spectroscopy, Sludyanka, Russia

INTRODUCTION

The tourmaline supergroup minerals are widespread, occurring in sedimentary, igneous, and metamorphic rocks (Dutrow and Henry 2011). They are important indicator minerals that can provide information on the compositional evolution of their host rocks, chiefly due to their ability to incorporate many elements (e.g., Novák et al. 2004, 2011; Agrosì et al. 2006; Lussier et al. 2011a; van Hinsberg et al. 2011; Bačík et al. 2012). However, the chemical composition of tourmalines is also controlled by short-range and long-range constraints (e.g., Hawthorne 1996, 2002; Bosi and Lucchesi 2007; Bosi 2010, 2011, 2013; Henry and Dutrow 2011; Skogby et al. 2012). Tourmaline supergroup minerals are complex borosilicates and their crystal structure and crystal chemistry have been extensively studied (e.g., Foit 1989; Hawthorne and Henry 1999; Bosi and Lucchesi 2007; Lussier et al. 2008, 2011b; Bosi 2008; Bosi et al. 2010; Filip et al. 2012). In accordance with Henry et al. (2011), the general formula of tourmaline may be written as: $XY_3Z_6T_6O_{18}(BO_3)_3V_3W$, where X ($\equiv {}^{[9]}X$) = Na^+, K^+, Ca^{2+}, $\square$ (= vacancy); Y ($\equiv {}^{[6]}Y$) = Al^{3+}, Fe^{3+}, Cr^{3+}, V^{3+}, Mg^{2+}, Fe^{2+}, Mn^{2+}, Li^+; Z ($\equiv {}^{[6]}Z$) = Al^{3+}, Fe^{3+}, Cr^{3+}, V^{3+}, Mg^{2+}, Fe^{2+}; T ($\equiv {}^{[4]}T$) = Si^{4+}, Al^{3+}, B^{3+}; B ($\equiv {}^{[3]}B$) = B^{3+}; W ($\equiv {}^{[3]}$O1) = OH^{1-}, F^{1-}, O^{2-}; V ($\equiv {}^{[3]}$O3) = OH^{1-}, O^{2-} and where, for example, T represents a group of cations (Si^{4+}, Al^{3+}, B^{3+}) accommodated at the [4]-coordinated T sites. The dominance of these ions at one or more sites of the structure gives rise to a range of distinct mineral species.

Recently, several new minerals of the tourmaline super-

---

* E-mail: ferdinando.bosi@uniroma1.it

0003-004X/14/0809–1767$05.00/DOI: http://dx.doi.org/10.2138/am.2014.4787

group were approved by the Commission on New Minerals, Nomenclature, and Classification (CNMNC) of the International Mineralogical Association (IMA). Among these are several oxy-tourmalines related by complete solid solution in the Al^{3+}-Cr^{3+}-V^{3+} subsystem: oxy-dravite, end-member formula $NaAl_3(Al_4Mg_2)(Si_6O_{18})(BO_3)_3(OH)_3O$ (IMA 2012-004a; Bosi and Skogby 2013), oxy-chromium-dravite, $NaCr_3(Cr_4Mg_2)(Si_6O_{18})(BO_3)_3(OH)_3O$ (IMA 2011-097; Bosi et al. 2012a); oxy-vanadium-dravite, $NaV_3(V_4Mg_2)(Si_6O_{18})(BO_3)_3(OH)_3O$ (IMA 11-E; Bosi et al. 2013a); vanadio-oxy-dravite, $NaV_3(Al_4Mg_2)(Si_6O_{18})(BO_3)_3(OH)_3O$ (IMA 2012-074; Bosi et al. 2014a); vanadio-oxy-chromium-dravite, $NaV_3(Cr_4Mg_2)(Si_6O_{18})(BO_3)_3(OH)_3O$ (IMA 2012-034; Bosi et al. 2014b).

Chromo-alumino-povondraite was originally approved as a new species by the IMA CNMMN in 2009 (no. 2009-088). Subsequent additional work connected with publication of the resultant paper showed that the chemical analysis associated with the original proposal was not reliable. Further work uncovered an appropriate sample with the requisite chemical composition for this species. Consultation with the Chair of CNMMN resulted in a new proposal that involved changing the holotype sample. The original approval of IMA 2009-088 was hence withdrawn on January 30, 2013 (Williams et al. 2013), and a new proposal was submitted and approved by the IMA-CNMNC (no. 2013-089). The holotype specimen (sample PR85v) is deposited in the collections of the Museum of Mineralogy, Earth Sciences Department, Sapienza University of Rome, Italy, catalog number 33069/1. A formal description of the new species chromo-alumino-povondraite is presented here, including a full characterization of its physical, chemical, and structural properties.

OCCURRENCE, APPEARANCE, PHYSICAL, AND OPTICAL PROPERTIES

The crystals of chromo-alumino-povondraite are green and occur in metaquartzites in the Pereval marble quarry, Sludyanka crystalline complex, Southern Baikal region, Russia (51°37′N 103°38′E). The Sludyanka complex underwent regional granulite facies metamorphism in the Early Ordovician (Kotov et al. 1997; Kovach et al. 2013). The Pereval quarry is the type locality (see Reznitsky et al. 2001 and Bosi et al. 2012a for a more detailed description) for natalyite, florensovite, kalininite, magnesiocoulsonite, oxy-vanadium-dravite, oxy-chromium-dravite, vanadio-oxy-chromium-dravite, vanadio-oxy-dravite, batisivite, oxyvanite, and cuprokalininite. Minerals associated with the holotype specimen are: dravite, oxy-chromium-dravite, oxy-dravite, quartz, calcite, chromphyllite, eskolaite, chromite, uvarovite, chromian phlogopite, and pyroxenes of the diopside-kosmochlor series, Cr-bearing tremolite, Cr-bearing titanite, Cr-bearing rutile, and pyrite, The host rocks (quartz-diopside) are Cr-V-bearing carbonate-siliceous sediments, metamorphosed to granulite facies and partly diaphtorized (Salnikova et al. 1998) to amphibolite facies (retrograde stage). Chromo-alumino-povondraite probably formed during the prograde stage (granulite facies). The crystals are euhedral, reaching up to 0.3 mm in length, and may be chemically zoned (for details, see Fig. 3 of Bosi et al. 2013a), but homogeneous crystals also occur.

The morphology of chromo-alumino-povondraite consists of elongated $\{10\bar{1}0\}$ and $\{11\bar{2}0\}$ prisms terminated by a prominent $\{0001\}$ pedion and small, minor $\{10\bar{1}1\}$ pyramidal faces. Crystals are green, with a pale-green streak, transparent, and display vitreous luster. They are brittle and show conchoidal fracture. The Mohs hardness is approximately 7½ (Reznitsky et al. 2001). The calculated density is 3.227 g/cm³. In transmitted light, chromo-alumino-povondraite is pleochroic with O = emerald green and E = pale yellowish green. Chromo-alumino-povondraite is uniaxial negative with refractive indices, measured by the immersion method using white light from a tungsten source, of $\omega = 1.745(5)$, $\varepsilon = 1.685(5)$. The mean index of refraction, density, and chemical composition lead to superior compatibility indices ($1 - K_p/K_c = 0.011$) (Mandarino 1976, 1981).

METHOD

General comment

The present crystal-structure refinement and electron-microprobe analyses were obtained from the same single crystal. However, complementary optical data, Fourier-transform infrared and optical-absorption spectra, refractive indices, and X-ray powder diffraction data were recorded on coexisting crystals. Small differ-

TABLE 1. Single-crystal X-ray diffraction data details for chromo-alumino-povondraite

Sample	PR85v
Crystal size (mm)	0.10 × 0.10 × 0.20
a (Å)	16.0277(2)
c (Å)	7.3085(1)
V (Å³)	1625.93(5)
Range for data collection, 2θ (°)	5–72
Reciprocal space range hkl	$-26 \le h \le 15$ $-26 \le k \le 26$ $-11 \le l \le 10$
Total number of frames	3265
Set of measured reflections	7819
Unique reflections, R_{int} (%)	1803, 2.02
Redundancy	8
Absorption correction method	SADABS
Refinement method	Full-matrix last-squares on F^2
Structural refinement program	SHELXL-97
Extinction coefficient	0.00057(8)
Flack parameter	0.05(2)
$wR2$ (%)	3.43
$R1$ (%) all data	1.68
$R1$ (%) for $I > 2\sigma(I)$	1.58
GooF	1.055
Largest diff. peak and hole ($\pm e^-/Å^3$)	–0.39 and 0.34

Notes: R_{int} = merging residual value; $R1$ = discrepancy index, calculated from F-data; $wR2$ = weighted discrepancy index, calculated from F^2-data; GooF = goodness of fit; diff. peaks = maximum and minimum residual electron density. Radiation, Mo$K\alpha$ = 0.71073 Å. Data collection temperature = 293 K. Space group $R3m$; Z = 3.

TABLE 2. Fractional atom coordinates and site occupancy for chromo-alumino-povondraite

Site	x	y	z	Site occupancies
X	0	0	0.22801(18)	$Na_{1.044(6)}$
Y	0.12380(2)	0.061898(10)	0.63723(5)	$Cr_{0.767(4)}$ $Mg_{0.233(4)}$
Z	0.297903(19)	0.261913(19)	0.60938(6)	$Cr_{0.280(2)}$ $Mg_{0.720(2)}$
B	0.10993(6)	0.21986(12)	0.4549(2)	$B_{1.00}$
T	0.190426(19)	0.18870(2)	0	$Si_{1.00}$
O1 (≡W)	0	0	0.7661(3)	$O_{1.00}$
O2	0.06037(4)	0.12074(8)	0.48900(15)	$O_{1.00}$
O3 (≡V)	0.25735(9)	0.12868(4)	0.51027(17)	$O_{1.00}$
O4	0.09256(4)	0.18511(9)	0.07144(16)	$O_{1.00}$
O5	0.18285(9)	0.09142(4)	0.09074(15)	$O_{1.00}$
O6	0.19226(6)	0.18294(6)	0.78002(12)	$O_{1.00}$
O7	0.28334(5)	0.28296(5)	0.07444(12)	$O_{1.00}$
O8	0.20763(6)	0.26830(6)	0.43859(13)	$O_{1.00}$
H3	0.2575(16)	0.1287(8)	0.395(3)	$H_{1.00}$

TABLE 3. Displacement parameters (Å^2) for chromo-alumino-povondraite

Site	U^{11}	U^{22}	U^{33}	U^{23}	U^{13}	U^{12}	U_{eq}/U_{iso}*
X	0.0212(5)	0.0212(5)	0.0186(7)	0	0	0.0106(2)	0.0203(4)
Y	0.00518(13)	0.00495(10)	0.00650(12)	−0.00037(4)	−0.00074(8)	0.00259(6)	0.00552(7)
Z	0.00424(12)	0.00464(12)	0.00442(11)	0.00026(8)	0.00002(8)	0.00207(10)	0.00450(7)
B	0.0065(5)	0.0073(6)	0.0083(6)	0.0005(5)	0.0003(2)	0.0036(3)	0.0072(3)
T	0.00567(13)	0.00524(12)	0.00609(13)	−0.00050(9)	−0.00042(10)	0.00266(10)	0.00570(7)
O1	0.0071(5)	0.0071(5)	0.0073(8)	0	0	0.0035(2)	0.0072(3)
O2	0.0066(3)	0.0048(4)	0.0083(5)	0.0006(3)	0.00029(17)	0.0024(2)	0.0068(2)
O3	0.0138(5)	0.0128(4)	0.0054(4)	0.00036(19)	0.0007(4)	0.0069(3)	0.0105(2)
O4	0.0085(3)	0.0174(6)	0.0087(5)	−0.0004(4)	−0.0002(2)	0.0087(3)	0.0106(2)
O5	0.0161(6)	0.0079(3)	0.0087(5)	0.0005(2)	0.0011(4)	0.0081(3)	0.0100(2)
O6	0.0104(3)	0.0080(3)	0.0055(3)	−0.0009(2)	−0.0004(3)	0.0052(3)	0.00773(14)
O7	0.0084(3)	0.0072(3)	0.0092(3)	−0.0005(3)	−0.0024(3)	0.0015(3)	0.00938(15)
O8	0.0055(3)	0.0094(4)	0.0173(4)	0.0031(3)	0.0010(3)	0.0033(3)	0.01093(16)
H3							0.016*

Note: Equivalent (U_{eq}) and isotropic (U_{iso}) displacement parameters; H-atom was constrained to have a U_{iso} 1.5 times the U_{eq} value of the O3 oxygen.

TABLE 4. Selected bond distances (Å) for chromo-alumino-povondraite

B-O2	1.3614(12)	*Y*-O1	1.9594(9)
B-O8^A (× 2)	1.398(2)	*Y*-O2^B (× 2)	2.0138(7)
<*B*-O>	1.374	*Y*-O3	2.0731(12)
		Y-O6^C (× 2)	1.9818(8)
T-O4	1.6267(5)	<*Y*-O>	2.004
T-O5	1.6420(5)		
T-O7	1.5957(7)	*Z*-O3	2.0296(6)
T^a-O6	1.6115(9)	*Z*-O6	1.9701(8)
<*T*-O>	1.619	*Z*-O8^E	1.9380(8)
		Z-O7^E	1.9839(8)
X-O2^{B,F} (× 3)	2.5390(14)	*Z*-O7^D	1.9504(8)
X-O4^{B,F} (× 3)	2.8126(13)	*Z*-O8	1.9519(9)
X-O5^{B,F} (× 3)	2.8127(13)	<*Z*-O>	1.971
<*X*-O>	2.694	O3-H	0.84(2)

Notes: Standard deviation in parentheses. Superscript letters: A = $(y - x, y, z)$; B = $(y - x, -x, z)$; C = $(x, x - y, z)$; D = $(y - x + 1/3, -x + 2/3, z + 2/3)$; E = $(-y + 2/3, x - y + 1/3, z + 1/3)$; F = $(-y, x - y, z)$. Transformations relate coordinates to those of Table 2.
[a] Positioned in adjacent unit cell.

ences in composition are likely to occur between these crystals, as well as minor variations in chemistry within the crystal population.

Single-crystal structural refinement

A representative fragment of the type specimen was selected for X-ray diffraction measurements on a Bruker KAPPA APEX-II single-crystal diffractometer, at Sapienza University of Rome (Earth Sciences Department), equipped with a CCD area detector (6.2 × 6.2 cm^2 active detection area, 512 × 512 pixels) and a graphite crystal monochromator, using Mo$K\alpha$ radiation from a fine-focus sealed X-ray tube. The sample-to-detector distance was 4 cm. A total of ca. 3265 exposures (step = 0.2°, time/step = 20 s) covering a full reciprocal sphere with a redundancy of about 8 was used. Final unit-cell parameters were refined using the Bruker AXS SAINT program for reflections with $I > 10\sigma(I)$ in the range $5° < 2\theta < 72°$. The intensity data were processed and corrected for Lorentz, polarization, and background effects with the APEX2 software program of Bruker AXS. The data were corrected for absorption using the multi-scan method (SADABS). The absorption correction led to a significant improvement in R_{int}. No violations of $R3m$ symmetry were noted.

Structural refinement was done with the SHELXL-97 program (Sheldrick 2008). Starting coordinates were taken from Bosi et al. (2004). Variable parameters were: scale factor, extinction coefficient, atom coordinates, site-scattering values, and atom-displacement factors. To obtain the best values of statistical indexes ($R1$, $wR2$), a fully ionized scattering curve for O was used, whereas neutral scattering curves were used for the other atoms. In detail, the occupancy of the *X* site was modeled by using the Na scattering factor, and both the *Y* and *Z* sites using Cr and Mg scattering factors. The *T* and *B* sites were modeled, respectively, with Si and B scattering factors and with a fixed occupancy of 1, because refinement with unconstrained occupancies showed no significant deviations from this value. Three full-matrix refinement cycles with isotropic-displacement parameters for all atoms were followed by anisotropic cycles until convergence was attained. No significant correlations over a value of 0.7 between the parameters were observed at the end of refinement. Table 1 lists crystal data, data-collection information, and refinement details; Table 2 gives the fractional atom coordinates and site occupancies; Table 3 gives the displacement parameters; Table 4 gives selected bond distances. (A CIF[1] is available.)

TABLE 5. Powder X-ray data for chromo-alumino-povondraite

I_{meas}, %	d_{meas}, Å	d_{calc}, Å	*h k l*
47	6.496	6.496	1 0 1
24	5.058	5.055	0 2 1
18	4.643	4.646	3 0 0
42	4.279	4.280	2 1 1
55	4.019	4.024	2 2 0
44	3.548	3.550	0 1 2
6	3.417	3.421	1 3 1
51	3.010	3.012	1 2 2
6	2.934	2.932	3 2 1
3	2.659	2.662	3 1 2
100	2.601	2.606	0 5 1
4	2.477	2.479	2 4 1
13	2.415	2.411	2 3 2
12	2.370	2.370	5 1 1
5	2.327	2.323	6 0 0
11	2.225	2.220	5 0 2
12	2.161	2.165	0 3 3
46	2.006	2.068	1 5 2
7	2.039	2.042	1 6 1
2	2.015	2.012	4 4 0
18	1.943	1.944	3 4 2
6	1.913	1.907	1 4 3
4	1.872	1.869	6 2 1
14	1.685	1.685	0 6 3
12	1.658	1.659	2 7 1
19	1.608	1.610	5 5 0
2	1.563	1.562	4 6 1
8	1.533	1.534	7 3 1

Note: Estimated errors in d_{meas}-spacing range from 0.01 Å for large *d*-values to 0.001 Å for small *d*-values.

X-ray powder diffraction

X-ray powder data were collected with a Bruker D8 Discover SuperSpeed micro-powder diffractometer with multi-wire 2D detector using a modified Gandolfi attachment (Cu$K\alpha$ radiation, $\lambda = 1.54178$ Å, 50 kV, 60 mA). Two 10 h frames were collected and merged; no internal standard was used. Data listed in Table 5 are indexed on $a = 16.095(17)$, $c = 7.341(9)$ Å.

Electron-microprobe analysis

Electron-microprobe analyses of the crystal used for X-ray diffraction refinement were obtained by wavelength-dispersive spectrometry (WDS mode) with a Cameca SX50 instrument at the "Istituto di Geologia Ambientale e Geoingegneria

---

[1] Deposit item AM-14-802, CIF. Deposit items are stored on the MSA web site and available via the *American Mineralogist* Table of Contents. Find the article in the table of contents at GSW (ammin.geoscienceworld.org) or MSA (www.minsocam.org), and then click on the deposit link.

TABLE 6. Chemical composition of chromo-alumino-povondraite

	wt%		apfu
SiO_2	34.06(08)	Si	5.96(6)
B_2O_3[a]	9.93	B	3.00
Al_2O_3	14.94(10)	Al	3.08(3)
Cr_2O_3	25.09(21)	Cr^{3+}	3.47(4)
V_2O_3	1.56(37)	V^{3+}	0.22(5)
Fe_2O_3[b]	0.10(2)	Fe^{3+}	0.014(3)
MgO	8.65(14)	Mg	2.26(4)
CaO	0.37(9)	Ca	0.07(2)
Na_2O	2.57(14)	Na	0.87(5)
K_2O	0.08(4)	K	0.017(8)
F	0.45(7)	F	0.25(4)
H_2O[a]	2.59	OH	3.02
–O=F	–0.19		
Total	100.20		

Notes: Errors for oxides are standard deviations (in parentheses) of 10 spot analyses. Standard errors for the atomic proportions (in parentheses) were calculated by error-propagation theory; apfu = atoms per formula unit.

[a] Calculated by stoichiometry.

[b] Calculated as Fe^{3+}.

(Rome, Italy), CNR," operating at an accelerating potential of 15 kV and a sample current of 15 nA, 10 μm beam diameter. Minerals and synthetic compounds were used as standards: wollastonite (Si, Ca), magnetite (Fe), rutile (Ti), corundum (Al), vanadinite (V), fluorphlogopite (F), periclase (Mg), jadeite (Na), K-feldspar (K), sphalerite (Zn), metallic Cr, Mn, and Cu. The overlap corrections and the PAP routine were applied (Pouchou and Pichoir 1991). The results (Table 6) represent mean values of 10 spot analyses. In accord with the very low concentration of Li in dravitic samples (e.g., Henry et al. 2011) and the crystallization environment of the studied sample (i.e., Cr-bearing metaquartzites), the Li_2O content was assumed to be insignificant. Mn, Zn, Cu, and Ti were below the detection limits (0.03 wt%) in the studied sample.

Infrared spectroscopy

A homogeneous chromo-alumino-povondraite crystal from the holotype material was measured by Fourier-transform infrared (FTIR) absorption spectroscopy in the wavenumber range 2000–5000 cm^{-1} to characterize OH absorption bands, using a Bruker Equinox 55 spectrometer equipped with a tungsten-halogen source and a CaF_2 beam-splitter. Polarized spectra with a resolution of 4 cm^{-1} were acquired parallel and perpendicular to the crystallographic **c**-axis direction using an IR microscope with a KRS-5 wire-grid polarizer and an MCT detector. The 26 μm thick doubly-polished crystal plate had been oriented parallel the **c**-axis by morphology and optical microscopy. As normally observed, it was not possible to thin the sample sufficiently to avoid off-scale absorption intensity for the strongest band (Fig. 1).

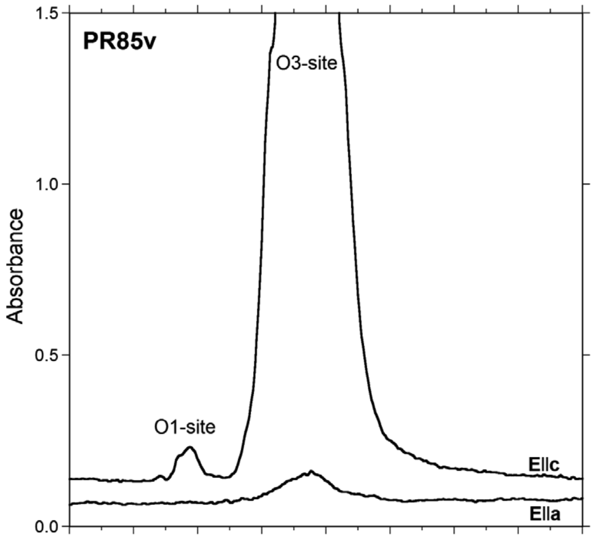

FIGURE 1. Polarized FTIR absorption spectra in the (OH)-stretching region of chromo-alumino-povondraite, vertically offset for clarity. Sample thickness 26 μm. The main band around 3530 cm^{-1} is truncated in the **c** direction due to excessive absorption. Spectral ranges expected for bands related to (OH) at the O1 and O3 anion sites are indicated.

Optical-absorption spectroscopy

Polarized, room-temperature optical-absorption spectra (OAS) were recorded on the same 26 μm thick crystal platelet used for the FTIR measurements. The spectra were measured in the range 300–1100 nm at a resolution of 1 nm using an AVASPEC-ULS2048X16 spectrometer attached via a 400 μm UV optical fiber to a Zeiss Axiotron UV-microscope. A 75 W Xenon arc lamp served as illuminating source and Zeiss Ultrafluar 10x lenses served as objective and condenser. A UV-quality Glan-Thompson prism with a working range from 250 to 2700 nm (40 000 to 3704 cm^{-1}) was used as a polarizer. The circular aperture was 64 μm in diameter. The wavelength scale of the spectrometer was calibrated against Ho_2O_3-doped and Pr_2O_3/Nd_2O_3-doped standards (Hellma glass filters 666F1 and 666F7) with an accuracy better than 15 cm^{-1} in the wavelength range 300–1100 nm. Recorded spectra were fitted using the Jandel PeakFit 4.12 software assuming Gaussian peak shapes.

RESULTS AND DISCUSSION

Determination of atomic proportions

In agreement with the structural-refinement results, the boron content was assumed to be stoichiometric in the chromo-alumino-povondraite sample (B^{3+} = 3.00 apfu). Both the site-scattering results and the bond lengths of *B* and *T* are consistent with the *B* site fully occupied by boron and no amount of B^{3+} at the *T* site (e.g., Hawthorne 1996; Bosi and Lucchesi 2007). The small contents of Fe were calculated as Fe^{3+}, on the basis of results of Bosi et al. (2013b). The (OH) content can then be calculated by charge balance with the assumption $T + Y + Z = 15.00$. The atomic proportions were calculated on this assumption (Table 6). The excellent match between the number of electrons per formula unit (epfu) derived from chemical and structural analysis supports this procedure, respectively: 265.6 and 266.3 epfu.

Site populations

The anion site populations in the studied sample follow the general preference suggested for tourmaline (e.g., Grice and Ercit 1993; Henry et al. 2011): the O3 site (V position in the general formula) is occupied by (OH), and the O1 site (W position in the general formula) is occupied by O^{2-}, $(OH)^{1-}$, and F^{1-}. The cation distribution at the *T*, *Y*, and *Z* sites was optimized by using a quadratic program to minimize the residuals between calculated and observed data (based on the chemical and structural analysis). Site-scattering values and octahedral and tetrahedral mean bond-distances (i.e., <*Y*-O>, <*Z*-O>, and <*T*-O>) were calculated as the linear contribution of each cation multiplied by its ideal bond-distance (Table 7). More details about the ideal distances as well as the optimization procedure may be found in Bosi et al. (2004) and Bosi and Lucchesi (2004, 2007). The robustness of this approach was confirmed by another optimization procedure (Wright et al. 2000), which led to very similar cation distributions (Table 7). This result represents another example of convergence of these two procedures to similar solutions for tourmaline (e.g., Bosi and Lucchesi 2007; Filip et al. 2012; Bosi et al. 2012a, 2013a; Bosi and Skogby 2013).

The final structural formula is as follows:

TABLE 7. Cation site populations (apfu), mean atomic numbers, and mean bond lengths (Å) for chromo-alumino-povondraite

Site	Site population	Mean atomic number		Mean bond length	
		Refined	Calculated	Refined	Calculated[a]
X	0.87 Na + 0.07 Ca + 0.04 □ + 0.02 K	11.49(7)	11.30		
Y	$2.29\ Cr^{3+} + 0.71\ Mg$ $(2.06\ Cr^{3+} + 0.66\ Mg + 0.23\ V^{3+} + 0.03\ Fe^{3+} + 0.03\ Al)$[b]	21.2(1)	21.2	2.004(1)	2.003
Z	$3.04\ Al + 1.54\ Mg + 1.18\ Cr^{3+} + 0.22\ V^{3+} + 0.01\ Fe^{3+}$ $(2.99\ Al + 1.59\ Mg + 1.42\ Cr^{3+})$[b]	15.4(1)	15.3	1.971(1)	1.964
T	5.96 Si + 0.04 Al	14[c]	14.00	1.619(1)	1.620
B	3 B	5[c]	5		

Note: apfu = atoms per formula unit.

[a] Calculated using the ionic radii of Bosi and Lucchesi (2007).

[b] Site populations optimized by the procedure of Wright et al. (2000).

[c] Fixed in the final stages of refinement.

TABLE 8. Bond valence calculations (valence units) for chromo-alumino-povondraite

Site	*X*	*Y*	*Z*	*T*	*B*	BVS
O1(W)		$0.50^{\times 3}\rightarrow$				1.50
O2	$0.14^{\times 3}\downarrow$	$0.45^{\times 2}\downarrow\rightarrow$			0.93	1.97
O3(V)		0.38	$0.39^{\times 2}\rightarrow$			1.16
O4	$0.07^{\times 3}\downarrow$			$0.99^{\times 2}\rightarrow$		2.05
O5	$0.09^{\times 3}\downarrow$			$0.95^{\times 2}\rightarrow$		1.99
O6		$0.49^{\times 2}\downarrow$	0.46	1.03		1.98
O7			0.48 0.44	1.08		2.00
O8			0.48 0.50		$1.02^{\times 2}\downarrow$	2.00
BVS	0.89	2.75	2.74	4.06	2.98	
MFV	1.03	2.76	2.74	3.99	3.00	

Note: BVS = bond valence sum; MFV = mean formal valence from site populations.

$$^{X}(Na_{0.87}Ca_{0.07}\square_{0.04}K_{0.02})_{\Sigma 1.00}\ ^{Y}(Cr^{3+}_{2.29}Mg_{0.71})_{\Sigma 3.00}\ ^{Z}(Al_{3.04}Mg_{1.54}Cr^{3+}_{1.18}V^{3+}_{0.22}Fe^{3+}_{0.01})_{\Sigma 6.00}\ [^{T}(Si_{5.96}Al_{0.04})O_{18}]\ (^{B}BO_3)_3\ ^{V}(OH)_3\ ^{W}[O_{0.73}F_{0.25}(OH)_{0.02}]_{\Sigma 1.00}.$$

The bond-valence analysis is consistent with the optimized structural formulas. Bond-valence sums (BVS), using the formula and bond-valence parameters from Brown and Altermatt (1985), are reported in Table 8. In this regard, note that the equation for the $^{W}(OH)$ calculation [reported by Bosi (2013), $^{W}(OH) = 2 - 1.01\ BVS(O1) - 0.21 - F$] yields an $^{W}(OH)$ value very close to that of the empirical formula: 0.03 and 0.02 apfu, respectively.

Name and crystal chemistry

The composition of the present sample PR85v is consistent with a tourmaline belonging to the alkali group, oxy-subgroup 3 (Henry et al. 2011): Na-dominant at the X position of the general formula of tourmaline $XY_3Z_6T_6O_{18}(BO_3)_3V_3W$ and oxygen-dominant at W with $O^{2-} > (OH+F)$. As Cr^{3+} is the dominant cation at Y and Al^{3+} is the dominant cation at Z, its end-member composition may be represented as $NaCr_3(Al_4Mg_2)Si_6O_{18}(BO_3)_3(OH)_3O$. Although tourmaline chemical compositions compatible with that of the studied sample were already reported in the literature (samples TMt6b, TMt3c, TMpr79f, and TM1p43e of Bosi et al. 2004), no samples have yet been formally defined as Cr^{3+}- and Al^{3+}-dominant at Y and Z (respectively). Therefore, the present tourmaline can be classified as a new species. Its closest end-member composition of a valid tourmaline species is that of oxy-dravite. The name chromo-alumino-povondraite is the same as the original name given in the 2009-088 proposal.

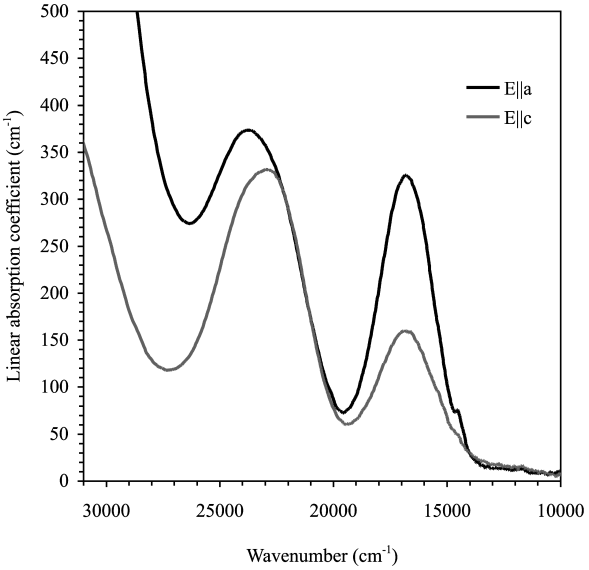

FIGURE 2. Polarized electronic absorption spectra for chromo-alumino-povondraite. Sample thickness 26 μm.

Although there exists a significant degree of Cr^{3+} and Mg disorder over the *Y* and *Z* sites, the structural formula of sample PR85v indicates a preference of Cr^{3+} for the *Y* site and Mg for the *Z* site. Al, on the other hand, is completely ordered at the *Z* site. The O1 site is dominated by O^{2-} with a significant concentration of F (0.25 apfu) and a minor concentration of (OH). The presence of only minor concentrations of (OH) at O1 (~0.02 apfu) are consistent with the observation of weak absorption bands at 3720 and 3760 cm^{-1} in the infrared spectrum (Fig. 1), i.e., the area typically ascribed to the O1 site (see below).

Infrared spectroscopy

Spectra recorded in polarized mode perpendicular and parallel to the crystallographic **c** axis show an intense broad band around 3530 cm^{-1} and two weak bands at 3720 and 3760 cm^{-1}, all strongly polarized in the **c** direction (Fig. 1). As it was not possible to thin the sample sufficiently to avoid off-scale absorption for the main band in the **c**-axis direction, any possible fine structure cannot be discerned. However, in line with previous studies (Bosi et al. 2012b, 2013b), the band can be related to the local arrangement ($^{Y}Cr^{3+}\ ^{Z}R\ ^{Z}R$)-O3, i.e., to the occurrence of (OH) at the V position of the tourmaline general formula (O3 site in the structure). The two weak bands at ca. 3720 and 3760 cm^{-1} are consistent with the minor concentrations of (OH) (ca. 0.02

TABLE 9. Selected properties of oxy-dravite, chromo-alumino-povondraite, and oxy-chromium-dravite

	Oxy-dravite	Chromo-alumino-povondraite	Oxy-chromium-dravite
a (Å)	15.9273(2)	16.0277(2)	16.0539(7)
c	7.2001(1)	7.3085(1)	7.3247(5)
V (Å³)	1581.81(4)	1625.93(5)	1634.86(15)
Space group	*R*3*m*	*R*3*m*	*R*3*m*
Optic sign	Uniaxial (–)	Uniaxial (–)	Uniaxial (–)
ω	1.650(5)	1.745(5)	1.765(5)
ε	1.620(5)	1.685(5)	1.715(5)
Color	Dark red	Green	Emerald green
Pleochroism	*O* = orange *E* = pink	*O* = emerald green *E* = pale yellowish green	*O* = dark green *E* = yellow green
Ref.[a]	(1)	(2)	(3)

[a] (1) Bosi and Skogby (2013); (2) this study; (3) Bosi et al. (2012a).

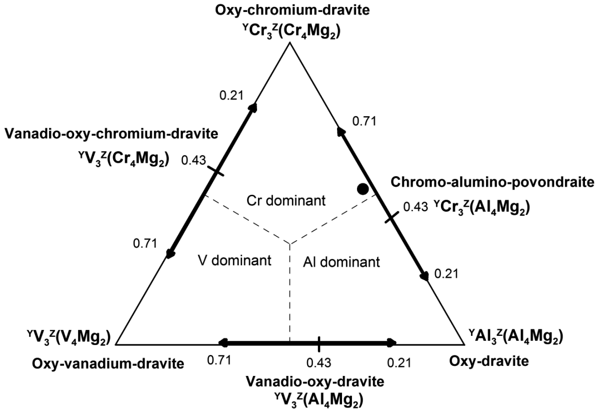

FIGURE 3. Ternary diagram of the V_{total}-Cr_{total}-Al_{total} subsystem for oxy-tourmaline $Na^{Y}(R^{3+})_3{}^{Z}(R^{3+}_4Mg_2)Si_6O_{18}(BO_3)_3(OH)_3O$. The solid black circle is the studied sample.

apfu) assigned to the W position (O1 site in the structure), and may be related to the local arrangements ^{Y}(Mg Mg Mg) and ^{Y}(Mg Mg R^{3+}) (cf. Gonzalez-Carreño et al. 1988; Bosi et al. 2012b, 2013b).

Optical-absorption spectroscopy

The optical spectra of chromo-alumino-povondraite show two broad absorption bands at ca. 435 and 590 nm, superimposed on an intense UV absorption edge (Fig. 2). These absorption bands are ascribed to spin-allowed *d-d* transitions in octahedrally coordinated Cr^{3+}, in accord with comparable bands at ca. 430 and 590 nm observed in spectra of Fe-bearing chromo-alumino-povondraite (Bosi et al. 2013b) as well as bands observed in spectra of other Cr-bearing tourmalines (Manning 1969; Taran et al. 1993; Ertl et al. 2008).

Relation to the other species

Chromo-alumino-povondraite [$NaCr_3(Al_4Mg_2)Si_6O_{18}(BO_3)_3(OH)_3O$] is related to oxy-dravite [$NaAl_3(Al_4Mg_2)Si_6O_{18}(BO_3)_3(OH)_3O$, in the ordered form] by the substitution $3Cr^{3+} \rightarrow 3Al$, and to oxy-chromium-dravite [$NaCr_3(Cr_4Mg_2)Si_6O_{18}(BO_3)_3(OH)_3O$] by the substitution $4Al \rightarrow 4Cr^{3+}$. The properties of these three tourmalines are compared in Table 9.

Figure 3 displays the ternary diagram of the V_{total}-Cr_{total}-Al_{total} system for oxy(O1)-tourmaline $Na^{Y}(R^{3+})_3{}^{Z}(R^{3+}_4Mg_2)Si_6O_{18}(BO_3)_3(OH)_3O$ (where R^{3+} = V, Cr, Al) showing the position of the studied sample and that of ideal chromo-alumino-povondraite. This species occurs between the series oxy-chromium-dravite and oxy-dravite, its compositional limits were calculated by Bosi et al. (2013b) at $^{Y+Z}(Cr_{1.5}Al_{5.5})$, corresponding to $Na^{Y}(Cr_{1.5}Al_{1.5})^{Z}(Al_4Mg_2)Si_6O_{18}(BO_3)_3(OH)_3O$ toward oxy-dravite, and $^{Y+Z}(Cr_5Al_2)$, corresponding to $Na^{Y}(Cr_3)^{Z}(Cr_2Al_2Mg_2)Si_6O_{18}(BO_3)_3(OH)_3O$ toward oxy-chromium-dravite. In a similar way, the compositional limits of vanadio-oxy-chromium-dravite and vanadio-oxy-dravite were inferred (Bosi et al. 2014a, 2014b).

IMPLICATIONS

The discovery of the new mineral chromo-alumino-povondraite provides new information on the crystal chemistry of the tourmaline supergroup. The current chemical data supports complete solid-solution of V^{3+}, Cr^{3+}, and Al in species of the tourmaline supergroup (Reznitsky et al. 2001; Bosi et al. 2004, 2013a, 2013b, 2014a, 2014b) showing that tourmaline with chemical compositions classified as chromo-alumino-povondraite can be either Al-dominant or Cr-dominant as a result of the compositional boundaries along the solid solution between Al and Cr.

ACKNOWLEDGMENTS

Chemical analyses were done with the kind assistance of Marcello Serracino to whom the authors express their gratitude. Leonid Reznitskii was supported by a grant from the Russian Foundation for Basic Research (project 13-05-00258). Frank Hawthorne was supported by a Canada Research Chair in Crystallography and Mineralogy and by Discovery, Equipment, and Major Installation grants of the Natural Sciences and Engineering Research Council of Canada, and by Innovation grants from the Canada Foundation for Innovation. The review of Darrell Henry and an anonymous referee as well as the handling of the AE Aaron Celestian is acknowledged.

REFERENCES CITED

Agrosì, G., Bosi, F., Lucchesi, S., Melchiorre, G., and Scandale, E. (2006) Mn-tourmaline crystals from island of Elba (Italy): Growth history and growth marks. American Mineralogist, 91, 944–952.

Bačík, P., Uher, P., Ertl, A., Jonsson, E., Nysten, P., Kanický, V., and Vaculovič, T. (2012) Zoned REE enriched dravite from a granitic pegmatite in Forshammar Bergslagen Province, Sweden an EMPA, XRD and LA–ICP-MS study. Canadian Mineralogist, 50, 825–841.

Bosi, F. (2008) Disordering of Fe^{2+} over octahedrally coordinated sites of tourmaline. American Mineralogist, 93, 1647–1653.

——— (2010) Octahedrally coordinated vacancies in tourmaline: a theoretical approach. Mineralogical Magazine, 74, 1037–1044.

——— (2011) Stereochemical constraints in tourmaline: from a short-range to a long-range structure. Canadian Mineralogist, 49, 17–27.

——— (2013) Bond-valence constraints around the O1 site of tourmaline. Mineralogical Magazine, 77, 343–351.

Bosi, F., and Lucchesi, S. (2004) Crystal chemistry of the schorl-dravite series. European Journal of Mineralogy, 16, 335–344.

——— (2007) Crystal chemical relationships in the tourmaline group: Structural constraints on chemical variability. American Mineralogist, 92, 1054–1063.

Bosi, F., and Skogby, H. (2013) Oxy-dravite, $Na(Al_2Mg)(Al_5Mg)(Si_6O_{18})(BO_3)_3(OH)_3O$, a new mineral species of the tourmaline supergroup. American Mineralogist, 98, 1442–1448.

Bosi, F., Lucchesi, S., and Reznitskii, L. (2004) Crystal chemistry of the dravite-chromdravite series. European Journal of Mineralogy, 16, 345–352.

Bosi, F., Balić-Žunić, T., and Surour, A.A. (2010) Crystal structure analysis of four tourmalines from the Cleopatra's Mines (Egypt) and Jabal Zalm (Saudi Arabia), and the role of Al in the tourmaline group. American Mineralogist, 95, 510–518.

Bosi, F., Reznitskii, L., and Skogby, H. (2012a) Oxy-chromium-dravite, $NaCr_3(Cr_4Mg_2)(Si_6O_{18})(BO_3)_3(OH)_3O$, a new mineral species of the tourmaline supergroup. American Mineralogist, 97, 2024–2030.

Bosi, F., Skogby, H., Agrosì, G., and Scandale, E. (2012b) Tsilaisite, $NaMn_3Al_6(Si_6O_{18})(BO_3)_3(OH)_3OH$, a new mineral species of the tourmaline supergroup from Grotta d'Oggi, San Pietro in Campo, island of Elba, Italy. American Mineralogist, 97, 989–994.

Bosi, F., Reznitskii, L., and Sklyarov, E.V. (2013a) Oxy-vanadium-dravite, $NaV_3(V_4Mg_2)(Si_6O_{18})(BO_3)_3(OH)_3O$: crystal structure and redefinition of the "vanadium-dravite" tourmaline. American Mineralogist, 98, 501–505.

Bosi, F., Skogby, H., Hålenius, U., and Reznitskii, L. (2013b) Crystallographic and spectroscopic characterization of Fe-bearing chromo-alumino-povondraite and its relations with oxy-chromium-dravite and oxy-dravite. American Mineralogist, 98, 1557–1564.

Bosi, F., Skogby, H., Reznitskii, L., and Hålenius, U. (2014a) Vanadio-oxy-dravite, $NaV_3(Al_4Mg_2)(Si_6O_{18})(BO_3)_3(OH)_3O$, a new mineral species of the tourmaline supergroup. American Mineralogist, 99, 218–224.

Bosi, F., Reznitskii, L., Skogby, H., and Hålenius, U. (2014b) Vanadio-oxy-chromium-dravite, $NaV_3(Cr_4Mg_2)(Si_6O_{18})(BO_3)_3(OH)_3O$, a new mineral species of the tourmaline supergroup. American Mineralogist, 99, 1155–1162.

Brown, I.D., and Altermatt, D. (1985) Bond-valence parameters obtained from a systematic analysis of the Inorganic Crystal Structure Database. Acta Crystallographica, B, 41, 244–247.

Dutrow, B.L., and Henry, D.J. (2011) Tourmaline: A geologic DVD. Elements, 7(5), 301–306.

Ertl, A., Rossman, G.R., Hughes, J.M., Ma, C., and Brandstätter, F. (2008) V^{3+}-bearing, Mg-rich strongly disordered olenite from a graphite deposit near Amstall, Lower Austria: A structural, chemical and spectroscopic investigation. Neues Jahrbuch für Mineralogie Abhandlungen, 184, 243–253.

Filip, J., Bosi, F., Novák, M., Skogby, H., Tuček, J., Čuda, J., and Wildner, M. (2012) Redox processes of iron in the tourmaline structure: example of the high-temperature treatment of Fe^{3+}-rich schorl. Geochimica et Cosmochimica Acta, 86, 239–256.

Foit, F.F. Jr. (1989) Crystal chemistry of alkali-deficient schorl and tourmaline structural relationships. American Mineralogist, 74, 422–431.

Gonzalez-Carreño, T., Fernandez, M., and Sanz, J. (1988) Infrared and electron micropobe analysis in tourmalines. Physics and Chemistry of Minerals, 15, 452–460.

Grice, J.D., and Ercit, T.S. (1993) Ordering of Fe and Mg in the tourmaline crystal structure: the correct formula. Neues Jahrbuch für Mineralogie, Abhandlungen, 165, 245–266.

Hawthorne, F.C. (1996) Structural mechanisms for light-element variations in tourmaline. Canadian Mineralogist, 34, 123–132.

——— (2002) Bond-valence constraints on the chemical composition of tourmaline. Canadian Mineralogist, 40, 789–797.

Hawthorne, F.C., and Henry, D. (1999) Classification of the minerals of the tourmaline group. European Journal of Mineralogy, 11, 201–215.

Henry, D.J., and Dutrow, B.L. (2011) The incorporation of fluorine in tourmaline: Internal crystallographic controls or external environmental influences? Canadian Mineralogist, 49, 41–56.

Henry, D.J., Novák, M., Hawthorne, F.C., Ertl, A., Dutrow, B., Uher, P., and Pezzotta, F. (2011) Nomenclature of the tourmaline supergroup minerals. American Mineralogist, 96, 895–913.

Kotov, A.B., Salnikova, E.B., Reznitskii, L.Z., Vasil'ev, E.P., Kozakov, I.K., Yakovleva, S.Z., Kovach, V.P., and Berezhnaya, N.G. (1997) Age of metamorphism of the Slyudyanka crystalline complex, Southern Baikal Area: U–Pb geochronology of granitoids. Petrology, 5, 338–349.

Kovach, V., Salnikova, E., Wang, K-L., Jahn, B-M., Chiu, H-Y., Reznitskiy, L., Kotov, A., Iizuka, Y., and Chung, S-L. (2013) Zircon ages and Hf isotopic constraints on sources of clastic metasediments of the Slyudyansky high-grade complex, southeastern Siberia: Implication for continental growth and evolution of the Central Asian Orogenic Belt. Journal of Asian Earth Sciences, 62, 18–36.

Lussier, A.J., Aguiar, P.M., Michaelis, V.K., Kroeker, S., Herwig, S., Abdu, Y., and Hawthorne, F.C. (2008) Mushroom elbaite from the Kat Chay mine, Momeik, near Mogok, Myanmar: I. Crystal chemistry by SREF, EMPA, MAS NMR and Mössbauer spectroscopy. Mineralogical Magazine, 72, 747–761.

Lussier, A.J., Hawthorne, F.C., Aguiar, P.M., Michaelis, V.K., and Kroeker, S. (2011a) Elbaite-liddicoatite from Black Rapids glacier, Alaska. Periodico di Mineralogia, 80, 57–73.

Lussier, A.J., Abdu, Y. Hawthorne, F.C., Michaelis, V.K., Aguiar, P.M., and Kroeker, S. (2011b) Oscillatory zoned liddicoatite from Anjanabonoina, central Madagascar. I. Crystal chemistry and structure by SREF and ^{11}B and ^{27}Al MAS NMR spectroscopy. Canadian Mineralogist, 49, 63–88.

Mandarino, J.A. (1976) The Gladstone-Dale relationship. Part I: derivation of new constants. Canadian Mineralogist, 14, 498–502.

——— (1981) The Gladstone-Dale relationship. Part IV: the compatibility concept and its application. Canadian Mineralogist, 19, 441–450.

Manning, P.G. (1969) Optical absorption spectra of chromium-bearing tourmaline, black tourmaline and buergerite. Canadian Mineralogist, 9, 57–70.

Novák, M., Povondra, P., and Selway, J.B. (2004) Schorl-oxy-schorl to dravite-oxy-dravite tourmaline from granitic pegmatites; examples from the Moldanubicum, Czech Republic. European Journal of Mineralogy, 16, 323–333.

Novák, M., Škoda, P., Filip, J., Macek, I., and Vaculovič, T. (2011) Compositional trends in tourmaline from intragranitic NYF pegmatites of the Třebíč Pluton, Czech Republic; electron microprobe, Mössbauer and LA-ICP-MS study. Canadian Mineralogist, 49, 359–380.

Pouchou, J.L., and Pichoir, F. (1991) Quantitative analysis of homogeneous or stratified microvolumes applying the model "PAP." In K.F.J. Heinrich and D.E. Newbury, Eds., Electron Probe Quantitation, p. 31–75. Plenum, New York.

Reznitsky, L.Z., Sklyarov, E.V., Ushchapovskaya, Z.V., Nartova, N.V., Kashaev, A.A., Karmanov, N.S., Kanakin, S.V., Smolin, A.S., and Nekrosova, E.A. (2001) Vanadiumdravite, $NaMg_3V_6[Si_6O_{18}][BO_3]_3(OH)_4$, a new mineral of the tourmaline group. Zapiski Vsesoyuznogo Mineralogicheskogo Obshchestva, 130, 59–72 (in Russian).

Salnikova, E.B., Sergeev, S.A., Kotov, A.B., Yakovleva, S.Z., Steiger, R.H., Reznitskiy, L.Z., and Vasil'ev, E.P. (1998) U-Pb zircon dating of granulite metamorphism in the Slyudyanskiy complex, Eastern Siberia. Gondwana Research, 1, 195–205.

Sheldrick, G.M. (2008) A short history of SHELX. Acta Crystallographica, A, 64, 112–122.

Skogby, H., Bosi, F., and Lazor, P. (2012) Short-range order in tourmaline: a vibrational spectroscopic approach to elbaite. Physics and Chemistry of Minerals, 39, 811–816.

Taran, M.N., Lebedev, A.S., and Platonov, A.N. (1993) Optical absorption spectroscopy of synthetic tourmalines. Physics and Chemistry of Minerals, 20, 209–220.

van Hinsberg, V.J., Henry, D.J., and Marschall, H.R. (2011) Tourmaline: an ideal indicator of its host environment. Canadian Mineralogist, 49, 1–16.

Williams, P.A., Hatert, F., Pasero, M., and Mills, S. (2013) New minerals, nomenclature modifications approved in 2013. Mineralogical Magazine, 77, 2695–2709.

Wright, S.E., Foley, J.A., and Hughes, J.M. (2000) Optimization of site occupancies in minerals using quadratic programming. American Mineralogist, 85, 524–531.

Manuscript received October 28, 2013
Manuscript accepted March 10, 2014
Manuscript handled by Aaron Celestian